silyl-iron complex, $CpFe(CO)(L)SiMe_3$ (L = CO, PPh_3, C_2H_4, or N_2).

Acknowledgment. We are grateful for support from the SERC, the EEC (Stimulation Contract No. SC1*0007), NATO (Grant No. 591/83), the Paul Instrument Fund of the Royal Society, the Donors of the Petroleum Research Fund, administered by the American Chemical Society, Perkin Elmer Ltd., and Nicolet Instruments Ltd. M.P. thanks the Nuffield Foundation for a Research Fellowship. We are also grateful to Dr. M. A. Healy, Mr. J. G. Gamble, Mr. J. M. Whalley, and Mr. D. Dye for their help and advice.

Application of Sensitivity Analysis to the Establishment of Intermolecular Potential Functions

Thomas S. Thacher,*,† A. T. Hagler,† and Herschel Rabitz‡

Contribution from Biosym Technologies, Inc., 10065 Barnes Canyon Road, San Diego, California 92121, and the Department of Chemistry, Princeton University, Princeton, New Jersey 08544. *Received February 20, 1990*

Abstract: The demands for accurate potential energy functions have increased synergistically with the sophistication and application of molecular modeling techniques. This study explored the utility of sensitivity analysis in the development and validation of potential energy functions. In particular, an intermolecular force field derived by fitting crystallographic data was examined using the methodology. The analysis was found to be very valuable in elucidating the relationship between the observables used in the fit and the resulting parameters. In addition, the method is shown to be useful as a quantitative probe for locating inaccuracies in the derived potential field.

The most common empirical methods for determining intermolecular potential energy expressions have proceeded in either a direct or an indirect manner.[1-6] In both methods the difference between a set of data and a corresponding set of values, calculated with use of an analytical expression for the intermolecular potential energy, is minimized by varying the potential parameters. The direct method involves generating a number of "data" points by performing ab initio calculations on a pair of molecules at different configurations. The "data" points usually considered are the intermolecular energies and the derivatives of the energy with respect to the atomic coordinates. In the indirect method the potential parameters are optimized to fit experimental crystal properties. While this approach is more satisfying than the former because the experimental potential surface is reproduced, the fitted points are restricted by the experimental geometry. This limitation is compounded by the symmetry of the crystal, which further constrains the region sampled on the potential energy surface. Additionally, many of the properties used in the optimization are a consequence of a summation over all different molecular interactions in the crystal. For example, the sublimation energy is found by summing over all the interactions between a central molecule and all other molecules within a given cutoff range. Thus, a least-squares fit to this observable reproduces the sum but not each individual interaction between the molecule and its neighbors. Because of this, it is important to simultaneously fit a variety of properties from crystals having different packing structures to ensure that the potential surface is adequately sampled.

In contrast to the indirect approach, the direct method requires a point-for-point fit of the data for each interaction geometry used in the optimization. Thus, it is more demanding that the indirect method and, as a result, the optimized parameters should be more defined. Unfortunately, the approach cannot always be applied because of limitations on computational time and the expense of generating the ab initio "data" points. Recently, efforts to develop methods to overcome this have been made. One method has been to replace the full calculations by calculations involving one molecule and a probe atom or diatom.[7] The other method has been to use the derivatives as "data".[8] The first method reduces the size of the calculation while the second reduces the number of calculations by using more information per calculation. Both approaches alleviate the computational problem somewhat and allow the approach to be used on larger systems. Nevertheless, the underlying problem, which is the lack of prior knowledge of where to calculate the "data" points to define the analytic function effectively with the fewest number of calculations, is not addressed.

This issue is related to a similar problem with the indirect method; that is, the relationship between the derived potential parameters and the crystal properties used in the optimization must be understood in order to efficiently define an analytic expression for the intermolecular potential. This study is part of an ongoing effort to systematically elucidate this relationship by using sensitivity analysis. This analysis has been shown to be useful for a wide variety of modeling problems in a number of different systems.[9-11] While the specifics of the application of sensitivity analysis to each of these problems differ, the common objective of the analysis is to use the technique to probe the dependence of the output on either the input or the mechanism that transforms the input into the output. When experimental data are used to optimize potential energy functions, the former objective is desired and the relevant quantities are the parametric sensitivity coefficients that quantify the sensitivity of the output to changes in the input parameters. In addition to the parametric coefficients, functional sensitivities are also of interest to determine the role of the *form* of the potential energy function in the optimization.

† Biosym Technologies, Inc.
‡ Princeton University.

(1) Pertsin, A. J.; Kitaigorodsky, A. I. *The Atom-Atom Potential Method: Application to Organic Molecular Solids*; Springer-Verlag: Berlin, 1987; Chapter 3.3, p 79.
(2) Miwa, Y.; Machida, K. *J. Am. Chem. Soc.* **1988**, *110*, 5183-5189.
(3) Bohm, H. J.; Ahlrichs, R.; Scharf, P.; Schiffer, H. *J. Chem. Phys.* **1984**, *81*, 1389-1395.
(4) Smit, P. H.; Derissen, J. L.; Van Duijneveldt, F. B. *Mol. Phys.* **1979**, *37*, 501-519.
(5) Williams, D. E.; Cox, S. R. *Acta Crystallogr.* **1984**, *B40*, 404-417.
(6) Warshel, A.; Lifson, S. *J. Chem. Phys.* **1970**, *53*, 582-594.
(7) Dinur, U.; Hagler, A. T. *J. Am. Chem. Soc.* **1989**, *111*, 5149-5151.
(8) Maple, J. R.; Dinur, U.; Hagler, A. T. *Proc. Natl. Acad. Sci. U.S.A.* **1988**, *85*, 5350-5354.
(9) Rabitz, H. *Comput. Chem.* **1981**, *5*, 267-180.
(10) Rabitz, H. *Chem. Rev.* **1987**, *87*, 101-112.
(11) Rabitz, H. *Science* **1989**, *246*, 221.

0002-7863/91/1513-2020$02.50/0

In this paper, the utility of sensitivity analysis will first be illustrated by calculating the elementary parametric sensitivity coefficients associated with the energy and rigid-body force and torque for a number of different configurations of the formamide dimer. By using these coefficients, information concerning the relationship between the interaction geometry of molecules and the underlying intermolecular potential energy expression may be gained. For example, the coefficients reveal the relative importance of the parameters in determining a specific configuration. This type of information is, of course, relevant in the optimization process since structural data are an observable used in the fit. When the coefficients are evaluated at the experimental structure, they can be used to locate parameters that cause deviations in the structure when it is minimized in the derived force field. In addition to these coefficients, the coefficients associated with the energy are also calculated to identify the parameters that most affect the energy.

In a second set of calculations, sensitivity coefficients for a set of 23 amide and carboxylic acid crystals were considered. By using a potential that had been optimized with respect to these crystals, the coefficients were evaluated at the experimental configuration as well as at the minimum energy configuration associated with the potential field. In addition to determining the parametric coefficients associated with the energy and the rigid-body torques and forces, we also examined the sensitivities of the lattice vectors to changes in the potential parameters. These sensitivities are of particular interest to polymer problems, since in many crystals these coefficients reflect the interactions of chains of molecules within the crystal.

Another class of derived sensitivities can be calculated from the elementary sensitivities[12,13] discussed above. These sensitivities are extremely useful in elucidating the interrelationship among parameters and/or observables. For example, they would be valuable indicators of the sensitivity of the calculation of a particular desired observable to the change in the other observables used to optimize the potential parameters. The utility of the derived coefficients is illustrated in the present crystal studies. The application of sensitivity analysis to the direct method, specifically to the question of efficiently locating "data" points on the ab initio surface, will be treated in a future paper. We want to emphasize that the purpose of the present work was to show the type and quality of information available through a sensitivity analysis. Implementation of the suggestions arising from the analysis will be treated in a later paper.

Theory

In a least-squares procedure, a merit function R is constructed from the summation of the squared weighted differences r_i between the calculated and experimental observables. Thus

$$R = \sum_i (\sigma_i r_i)^2 = \sum_i (\sigma_i (O_i^c[V(x,\alpha)] - O_i^e))^2 \tag{1}$$

where the summation extends over all observables and O_i^c is the theoretically calculated ith observable, which depends on the chosen potential form V. The latter potential depends on the vectors of atomic coordinates x and parameters α. Similarly, O_i^e is the "experimental" data being used as input; the latter data might truly have been measured in a laboratory, as for the present calculations, or obtained by ab initio energy calculations. The contribution of a particular observable to the total sum of squares is controlled by the weight σ_i. It is assumed that a form for the potential has been chosen and that the task is to determine the parameter vector α. This objective is achieved by minimizing R, which in turn leads to solving the set of equations

$$\partial R/\partial \alpha_j = 0 \tag{2}$$

for the vector of potential parameters α. In practice, the gradients may not exactly vanish, so that convergence to an optimal set of parameters is assumed when the gradients $\partial R/\partial \ln \alpha_j$ are small with respect to the value of the merit function.

Equation 2 implies the existence of a relationship between the potential parameters α and the chosen types of data O_i^e. This relationship can be made apparent by again differentiating eq 2 to produce the sensitivities $\partial \alpha_m/\partial O_k^e$ that satisfy the equation

$$\sum_m \left(\frac{\partial^2 R}{\partial \alpha_j\, \partial \alpha_m}\right)\left(\frac{\partial \alpha_m}{\partial O_k^e}\right) = -\left(\frac{\partial^2 R}{\partial \alpha_j\, \partial O_k^e}\right) \tag{3}$$

Here, $\partial R/(\partial \alpha_j\, \partial \alpha_m)$ may be recognized as a generalized Hessian associated with the residual R. Although it may not be entirely evident at this point, the structure of eq 3 is inherent to all types of sensitivity analysis found throughout the sensitivity literature on other applications. In general, the equations of sensitivity analysis are driven by a Hessian or Jacobian with an inhomogeneity that depends on the particular variable being probed.

In order to perform a least-squares fit of the crystal properties, the derivatives of the residuals r_i with respect to the parameters are routinely calculated.[14] As a result, the elements $\partial O_k/\partial \alpha_m$ have arisen in previous optimization studies.[15] However, in these studies the use of the coefficients has been rather limited in scope because they have been treated as byproducts of the optimization and not as quantities of fundamental interest. Here, we will focus on these and related coefficients to emphasize their physical significance in guiding potential optimization.

Methods

The form of the potential function that was optimized and used in the minimizations was a Lennard-Jones 6–12 plus coulombic interaction

$$v_{ij} = \frac{A_{ij}}{x_{ij}^{12}} - \frac{B_{ij}}{x_{ij}^{6}} + \frac{q_i q_j}{x_{ij}} \tag{4}$$

where i and j label a pair of atoms. The A_{ij} coefficients represent the repulsive contribution due to the overlapping electron clouds of filled shells while the B_{ij} coefficients are the longer-ranged dispersive terms due to induced dipole–induced dipole interactions.[16] The last term, describing the electrostatic interaction, is characterized by the usual product partial charges q_i. During the optimization the cross coefficients ($i \neq j$) are not explicitly varied. Instead, atomic parameters A_i and B_i, defined respectively as the square roots of A_{ii} and B_{ii}, are used, and the cross coefficients are determined as the product of these atomic parameters. For example, $A_{ij} = A_i \times A_j = (A_{ii} \times A_{jj})^{1/2}$ and similarly for B_{ij}. While the construction of the cross terms from the atomic parameters (i.e., the diagonal elements) represents a constraint on the optimization, it significantly reduces the number of repulsive and dispersive parameters that must be optimized: If n is the number of atom types, then the number of parameters will decrease from $n(n+1)/2$ to n. This reduction, in turn, greatly facilitates implementation of the optimization since it leads to a substantial increase in the ratio of experimental observables to parameters. Because one of the objectives of the present calculations was to associate the sensitivity of observable quantities with the underlying atomic structure, the relevant potential parameters should correspond to the physical characteristics of the structure. In this case a better choice of parameters would be the van der Waals radii r^*_i and atomic well depths ϵ^*_i. These parameters are related to the atomic pair A and B coefficients of the previous expression by the following relation

$$A_{ij} = \epsilon_i \epsilon_j (r^*_i r^*_j)^{12} \tag{5}$$

$$B_{ij} = 2\epsilon_i \epsilon_j (r^*_i r^*_j)^{6} \tag{6}$$

where the more common van der Waals diameter and atomic pair well depth are given by the quantities $r^*_{ij} = r^*_i r^*_j$ and $\epsilon_{ij} = \epsilon_i \epsilon_j$, respectively. The use of a geometric average for the diameter in lieu of an arithmetic one follows from the validity of constructing the mixed parameters A_{ij} and B_{ij}, where $i \neq j$, in eq 1 from the geometric average of the unmixed terms.

The parametric sensitivities with respect to the latter set can be derived from the former by the use of the chain rule and the above expressions, i.e.

$$\frac{\partial V_{ij}}{\partial r^*_i} = 12\epsilon_i r^{*11}_i \frac{\partial V_{ij}}{\partial A_i} + 6\sqrt{2}\epsilon_i r^{*5}_i \frac{\partial V_{ij}}{\partial B_i} \tag{7}$$

and

$$\frac{\partial V_{ij}}{\partial \epsilon_i} = r^{*12}_i \frac{\partial V_{ij}}{\partial A_i} + \sqrt{2} r^{*6}_j \frac{\partial V_{ij}}{\partial B_i} \tag{8}$$

(12) Rabitz, H.; Kramer, M.; Dacol, D. *Annu. Rev. Phys. Chem.* **1983**, *34*, 419–461.
(13) Eslava, L. A.; Eno, L.; Rabitz, H. *J. Chem. Phys.* **1980**, *73*, 4998–5012.
(14) Fletcher, R. *Practical Methods of Optimization*; John Wiley and Sons: New York, 1980; Chapter 6.
(15) Hagler, A. T.; Huler, E.; Lifson, S. *J. Am. Chem. Soc.* **1974**, *96*, 5319–5327.
(16) Hirshfelder, J. O.; Curtiss, C. F.; Bird, R. B. *Molecular Theory of Gases and Liquids*; Wiley: New York, 1954.
(17) Bradley, R. S.; Cotson, S. *J. Chem. Soc.* **1953**, *1953*, 1684.

Table I. Intermolecular Potential, Bond Increment, and van der Waals Parameters

(a) Intermolecular Potential Parameters for Carboxylic Acids and Amides

atom type	description
c′	carbonyl carbon in carboxylic acids and amides
o′	carbonyl oxygen in carboxylic acids and amide
o	hydroxyl oxygen in carboxylic acid
ho	hydroxyl hydrogen in carboxylic acid
n	nitrogen in primary amide
n_1	nitrogen in secondary amide
hn	hydrogen bonded to nitrogen in primary or secondary amide
c	aliphatic carbon
h	hydrogen bonded to aliphatic carbon

(b) Bond Increment Parameters

bond[a]	increment	bond[a]	increment	bond[a]	increment
$\delta_{c'o'}$	0.38	δ_{hnn_1}	0.28	$\delta_{c'h}$	−0.18
δ_{hnn}	0.41	δ_{hoo}	0.35	δ_{hoo}	0.35
		δ_{ch}	−0.12		

(c) van der Waals Parameters

atom	radius, r^*_i (Å)	well-depth, ϵ_i (kcal/mol)
c′	4.00	0.148
o′ (o)	3.15	0.227
n (n_1)	3.93	0.167
h	3.30	0.013
hn (ho)	0.00	0.00
c	3.39	0.039

[a] $\delta_{ij} = -\delta_{ji}$. [b] Atom types in parentheses are assumed to have equivalent parameters.

As in eq 1, the electrostatic term is represented by the coulombic interaction of the atomic-centered partial charges. Instead of optimizing these quantities explicitly, the expression is recast in terms of bond increments δ_{ij}. This parameter characterizes the increment of charge on atom i from the bond between atoms i and j. Thus, the partial charge on atom i is written as

$$q_i = \sum_j \delta_{ij} \tag{9}$$

where the sum is over all bonds emanating from atom i. The use of the latter quantities in the optimization has the advantage of removing the need to explicitly constrain the partial charges so that electroneutrality is conserved, i.e.

$$\sum_i^n q_i = 0$$

where n is the number of atoms in the molecule. In addition it is believed that these quantities may be more transferable than partial charges since the bonding environment around the central atom is explicitly considered.

The set of parameters that were optimized for the amide and acid crystals and used in the present calculations is listed in Table I. It should be noted that the order of the atom pairs of the bond increments defines the sign of the increment; i.e., $\delta_{ch} = -\delta_{hc}$. Although a particular parametrization is employed above for pragmatic reasons, we emphasize that the sensitivity analysis tools are quite general and may be applied to other suitable potential forms.

In the following section the calculations involving the formamide dimer are presented first, because the analysis is straightforward which makes it easier to demonstrate the utility of the method. In the second part, the analysis of the crystals is presented both in terms of individual crystals as well as with respect to the collection of crystals. The former analysis illustrates the ability of the sensitivity coefficients to differentiate between specific types of interactions, while the second uses the analysis to probe the optimization as a whole. In this regard, it should be noted that the technique provides a tremendous amount of information which, by using appropriate averages, allows the analysis to be carried out at several different levels. We will generally emphasize the broad qualitative trends of the results as they are most interesting at this initial development of intermolecular potential sensitivity analysis. Exceptions to these trends can be found in the results and they may be of special interest in future work. Finally, the last section concludes with a discussion of future applications of the analysis to other issues that are important for molecular mechanics and dynamics simulations.

Results

I. Dimer Calculations. The four molecules in the formamide crystal unit cell pack according to Figure 1. As seen in the figure, pairs of formamide molecules, labeled AB and A′B′, associate to form dimers with two symmetric hydrogen bonds between the amide hydrogen and the carbonyl oxygen. These dimers are then held together with four hydrogen bonds of the same type per dimer. For the calculations, the initial configuration of the isolated dimer was taken to be the one found experimentally in the crystal, except that the distance between the carbonyl carbons was arbitrarily set at 6.0 Å. This distance was chosen to be sufficiently far away from the equilibrium configuration to allow the minimizer to step though a number of significantly different configurations before converging to the relaxed structure. The initial configuration was then relaxed in the force field assuming only rigid-body motion; i.e., the internal degrees of freedom of the molecule were fixed so that only the relative orientation of and intermolecular distance between the molecules were permitted to vary. The sequence of configurations associated with each step of the minimization is shown in Figure 2, and the changes in the intermolecular distances, angles, and energy are shown in Table II along with the changes in the rigid-body force and torque.

The objective of this calculation was to illustrate the variation in sensitivity coefficients with configurational changes. In addition, the results demonstrated how the sensitivities can be used to identify the relative effect that a particular parameter or type of interaction has on the stability of a specific configuration. This objective is particularly important to the development of force fields, because the first step in the validation of a derived field is the relaxation of experimental crystal structures in the field. The sensitivity coefficients that are calculated at the experimental configuration can be used to determine which interactions cause shifts in the experimental configuration. The variations in the

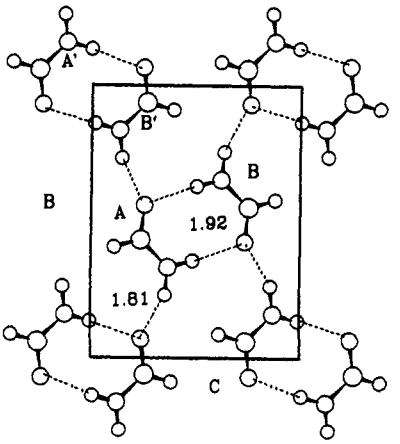

Figure 1. Experimental crystal structure for formamide viewed along the **a** axis. Molecular pairs AB and A′B′ form symmetric hydrogen bond dimers that are connected via the interdimer hydrogen bond.

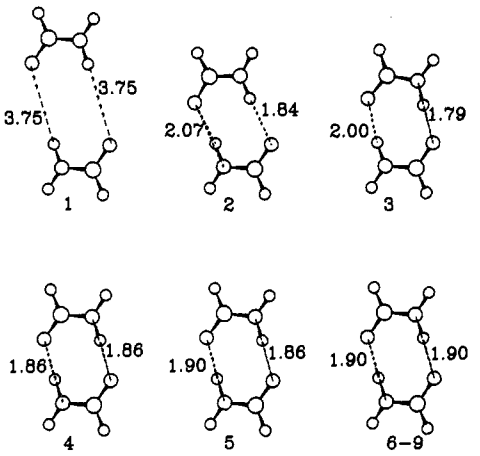

Figure 2. Formamide dimer configuration as a function of minimization iteration. Configurations 6–9 are represented as one configuration since the scale of the figure does not reflect the differences in the variables listed in Table II.

Table II. Intermolecular Distances, Angles, and Energies for the Formamide Dimer during Minimization

	distance (Å)		angle (deg)	energy (kcal/mol)[a]			force[b]			
iteration	c′···c′	c′···ho	n–hn···ho′	ele	vdw	total	torque	*x*	*y*	mod
1	6.0	3.75	178.66	−2.29	−0.39	−2.68	−1.07	2.00	0.034	2.00
2	4.19	1.84	174.78	−10.88	0.44	−10.44	9.16	−0.323	1.78	1.80
3	4.13	1.79	174.91	−11.65	1.23	−10.42	10.4	−3.74	−1.66	4.09
4	4.11	1.86	175.9	−12.27	1.44	−10.83	1.84	−3.99	−0.724	4.06
5	4.13	1.86	175.68	−12.10	1.16	−10.94	1.23	−2.46	0.069	2.465
6	4.15	1.90	179.20	−11.80	0.82	−10.99	0.447	−0.994	−0.072	0.99
7	4.15	1.90	179.26	−11.80	0.81	−10.99	−0.032	−0.946	−0.072	0.95
8	4.15	1.90	179.21	−11.79	0.80	−10.99	−0.026	−0.911	−0.022	0.911

[a] ele and vdw denote the electrostatic and van der Waals components of the total energy. [b] *x* and *y* represent the orthogonal rigid-body force components in the plane of the dimer, and mod is the modulus of these components ($x^2 + y^2$).

sensitivities during minimization are also important, because they are useful in uncovering particular interactions or types of interactions that guide the minimization along the potential energy surface. Unlike the initial and final configurations, the configurations generated during the minimization are dependent on the type of minimizer used. Thus, the set of sensitivities and the information uncovered by these sensitivities are dependent on the type of minimizer used. This issue has a direct connection to the use of sensitivity analysis to probe the potential interaction that determines a molecular dynamics trajectory. The latter application, which potentially has a very important role in probing the relationships relating to structure–function issues as well as to the potential energy question, is currently being pursued.

The sensitivity coefficients for the energy and rigid-body force and torque with respect to the bond increments are shown in Figure 3. The energy sensitivity coefficients are normalized with respect to the parameters and the energy, so that the plotted coefficients are $\partial \ln V/\partial \ln \delta_j$. The rigid-body force and torque coefficients were normalized with respect to the parameters only because the torque and force vanish at the minimum energy configuration. Thus, the listed coefficients are $\partial F/\partial \ln \delta_j$ and $\partial T/\partial \ln \delta_j$, respectively. The normalization allows the comparison to be made between coefficients associated with the same observables but different parameters, since these derivatives are interpreted as the change in observable O due to a fractional change in parameter α. As expected, relatively large changes in the sensitivities were observed for the first six configurations, where there are significant structural changes in the dimer. The sensitivity of the energy is larger for $\delta_{c'o'}$ and δ_{hnn} than for $\delta_{c'h}$. This result follows from the structure of the dimer, which derives a large part of its stabilization from the dipole interaction between the c′–o′ and n–hn bonds. In a one-dimensional system the $1/r$ relationship between the coefficients associated with the energy V and the force $F = -\Delta V$ are transparent in a comparison of the coefficients. However, in these calculations the dimer is planar, so that the force on an atom is generally not directed solely along one component and, as a result, the sensitivity effects are more subtle. Nevertheless, the similarity between the force and energy coefficients for δ_{hnn} and $\delta_{c'o'}$ is noticeable. In contrast, the sensitivities associated with the torque differ considerably from both the energy and force sensitivities. These differences are important in terms of optimizing a set of parameters with respect to these observables, because they indicate the relative importance of the observables in defining a particular parameter. A large sensitivity coefficient implies that small changes in the parameter of interest, with all others held constant, will give rise to large changes in the observable. Thus, if that observable is used in the optimization it will lead to a better-defined parameter. As an example consider the sensitivities associated with the c′–h bond increment. Although the sensitivity $\partial T/\partial \ln \delta_{c'h}$ (Figure 3C) is smaller than $\partial T/\partial \ln \delta_{hnn}$ it is comparable to the other sensitivities associated with this observable. This should be contrasted with the $\partial \ln V/\partial \ln \delta_{c'h}$ and $\partial F/\partial \ln \delta_{c'h}$ sensitivities (parts A and B in Figure 3, respectively), which are much smaller than the other remaining sensitivities associated with the energy and rigid-body force. Thus, inclusion of the condition of vanishing torques as an observable will define $\delta_{c'h}$ more than inclusion of the energy or rigid-body force.

The overall trend of the energy and force sensitivity coefficients

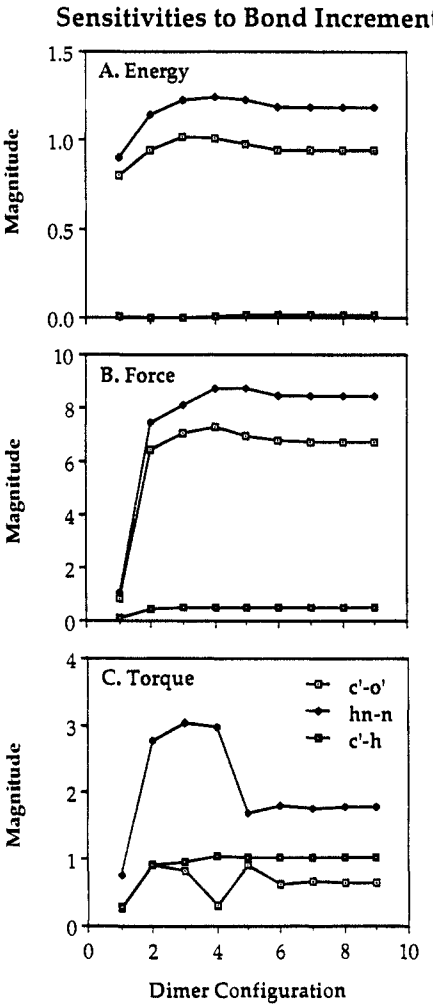

Figure 3. Variation in elementary sensitivities of the energy, torque, and force with respect to the bond increments: (A) $\partial \ln V/\partial \ln \delta_{c'o'}$, $\partial \ln V/\partial \ln \delta_{hnn}$, and $\partial \ln V/\partial \ln \delta_{c'h}$; (B) $\partial F/\partial \ln \delta_{c'o'}$, $\partial F/\partial \ln \delta_{hnn}$, and $\partial F/\partial \ln \delta_{c'h}$, (C) $\partial T/\partial \ln \delta_{c'o'}$, $\partial T/\partial \ln \delta_{hnn}$, and $\partial T/\partial \ln \delta_{c'h}$.

is an initial increase followed by a leveling off or decrease in magnitude as the distance between the dimers decreases. It can also be observed that the sensitivities go through a maximum at the third or fourth configuration. This correlates with the distance between the dimers, which in the third and fourth configuration include hydrogen bond distances of 1.79 and 1.86 Å, respectively. The relative magnitude of the coefficients for the energy and force observables is quantitatively the same for the minimized configuration: the ratio of the force sensitivities to the bond increments is 0.78:1.0:0.05 for $\delta_{c'o'}$, δ_{hnn}, and $\delta_{c'h}$ and 0.79:1.0:0.015 for the corresponding energy sensitivities. This result suggests that changes in these parameters affect the observables in a parallel manner. Because of this, use of both observables in the optimization will not define these parameters any better than if only one of the observables is used.

Table III. Intermolecular Distances Involving the Carbonyl Oxygen of Molecules A and B of the Formamide Dimer

	iteration 3		iteration 4	
	A	B	A	B
o′···c′	3.57	3.68	3.64	3.65
o′···h	4.65	4.77	4.72	4.72
o′···o′	3.51	3.51	3.58	3.58
o′···n	2.80	2.99	2.86	2.87
o′···hn	3.43	3.68	3.49	3.50
o′···hn	1.79	2.00	1.86	1.86

The sensitivities associated with the torque show a much different behavior than the previous types of sensitivities. As with the energy and force, the sensitivity to the hnn bond increment is the greatest. However, in this case the sensitivity to the $\delta_{c'h}$ increment is greater than that to $\delta_{c'o'}$. Furthermore, the sensitivity goes through a minimum at the fourth configuration for the c′o′ bond increment. This minimum is a result of a balance of forces on the carbonyl oxygen atoms o′ in both dimer molecules. As shown in Table III, the o′ intermolecular distances for both molecules in the dimer are virtually identical for the fourth configuration. For example, the rms deviation in the intermolecular distances is 0.167 for configuration 3 as compared to 0.007 for configuration 4. The lack of sensitivity of the torque to changes in this bond increment, implied by the relatively small sensitivity coefficient, provides an especially clear example of how the coefficients can be used to probe the relative importance of parameters in determining a specific observable. In this case they demonstrate that changes in $\delta_{c'o'}$ will not change the torque significantly. Thus, if this configuration were the experimental structure used in the optimization, use of the torque as an observable would not contribute to any refinement in the parameter.

In many modeling problems one is interested in determining which forces either stabilize a particular configuration or cause a structural change in the configuration. Similarly, when fitting a potential field to experimental observables that depend on the underlying structure, the goal is to locate those interactions that promote deviations in the calculated structure from the experimental one. Sensitivity analysis can be used to address these concerns by calculating the coefficients $\partial\chi^{eq}/\partial\alpha$, where χ^{eq} represents the atomic coordinates of the energy-minimized structure in the former case or the experimental structure in the latter case. Parameters that significantly affect the configuration are then located by scanning the coefficients for large values. This type of information is also contained in the sensitivities associated with the rigid-body force and torque. A large sensitivity coefficient indicates that this particular parameter (or equivalently, interaction) contributes to a shift in the structure. As an illustration of this property, the sensitivities of the minimized dimer configuration are shown in Table IV. In this case the results reveal that the torque will be affected more by incremental changes in $\delta_{c'h}$ than will be the rigid-body force or energy. Thus, alterations in this parameter will cause one molecule to rotate relative to the other with only a relatively small impact on the intermolecular energy or the distance between the molecules. Indeed, if the increment is increased by 50% to −0.25, the torque increases from −0.026 to 0.88, while the energy decreases by only 0.07% and the rigid-body force increases by 30.8%.

II. Crystal Calculations. The lattice energy of a crystal, defined as the intermolecular energy per unit cell, is written as

$$V = \sum_{ij} V(|r_{ij}|) + \sum_{m}\sum_{ij} V(|r_{ij} + ma|) \qquad (10)$$

where the summation in the first term is over all intermolecular pairs of atoms within a central basic unit cell. The second term represents the contribution to the lattice energy from the surrounding unit cells. The first sum in this latter term extends over all unit cells in the crystal, excluding the basic unit cell, and the second sum is over all pairs of atoms in the unit cell. In order to make the calculations feasible, the number of interactions in the sum is limited by a cut-off distance beyond which the contribution to the energy from an interaction is assumed to be negligible. In the present study a cut-off distance of 12.0 Å was employed. To clarify the lattice vector notation used in this study, the Cartesian components of the vectors are written as a vector a that is related to the crystallographic axes **a**, **b**, and **c** by $\mathbf{a}^T = [\mathbf{a},\mathbf{b},\mathbf{c}]$.

Table IV. Elementary Sensitivities $\partial \ln V_i/\partial \ln \alpha_j$, $\partial F_i/\partial \ln \alpha_j$, and $\partial T_i/\partial \ln \alpha_j$ for the Final Minimum Energy Configuration of the Formamide Dimer

parameter α_j	observable: energy, V (kcal/mol)	force, F (kcal/(Å mol))	torque, T (kcal/(rad mol))
$\delta_{c'o'}$	0.943	6.736	0.650
δ_{hnn}	1.19	8.45	1.77
$\delta_{c'h}$	0.018	0.503	1.02
$r_{c'}$	0.119	8.59	33.20
$\epsilon_{c'}$	0.080	0.453	0.415
$r_{o'}$	1.48	50.77	0.631
$\epsilon_{o'}$	0.107	7.38	0.492
r_n	2.24	72.06	13.28
ϵ_n	0.007	0.052	0.005

Beginning with the experimental configuration, the minimal energy configuration for the intermolecular potential was found by allowing all nine Cartesian components of the lattice vectors, as well as the relative distances and orientations between the first molecule in the unit cell and all other molecules in the unit cell, to change. The sensitivity coefficients associated with the lattice energy, the rigid-body force, and torque were then calculated for both the initial (experimental) and final minimized crystal structures. In order to reduce the number of coefficients associated with the latter two observables, only the root-mean-square sensitivities are reported for the torque and force: i.e., the quantity

$$\left[z^{-1} \sum_{i}^{z} \left(\frac{\partial O_i}{\partial \ln \alpha_j} \right)^2 \right]^{1/2}$$

where z is the number of molecules per unit cell. While this averaged quantity reduces the amount of information provided by the analysis, the general behavior of the unaveraged sensitivities is preserved. The analysis of the sensitivity coefficients is partitioned into two sections. The first section demonstrates the type of information obtained by considering the *elementary* sensitivities of individual crystals. This information is particularly useful in determining the types of interactions that are important in the optimization, as well as in locating deficiencies in the potential. In the second part, the elementary sensitivities obtained as averages over the sets of amide and carboxylic acid crystals are considered. The latter quantities are relevant in a more global analysis of the relationship between the crystals including in the training set and the resulting optimized parameters. The utility of sensitivity analysis for probing this relationship is explored further in this part through calculation of a class of *derived* sensitivities.

A. Elementary Sensitivities. The studied crystals are listed in Table V along with relevant crystallographic information, and the sensitivities calculated at the experimental and energy-minimized structures for the amide crystals are displayed in Figures 4–7. The magnitude of the coefficient is plotted along the abscissa while the number of the crystal (Table V) is given by the ordinate. The carboxylic acid crystals are not shown, since the trends shown in the figures are representative also for them.

With the exception of the unit cell vector sensitivities, the coefficients did not in general change at a *qualitative* level when the crystals were minimized. There were some exceptions to this trend as witnessed by a marked change in the sensitivity of the energy to the van der Waals radius for the unmethylated and methylated diketopiperazine (crystals 8 and 9, respectively). In these cases the sensitivities shifted significantly due the relief of repulsive contacts when the crystal is minimized. The qualitative differences observed in the coefficients evaluated at the experimental and minimized configurations for the unit cell vectors were most likely due to the harmonic approximation used to obtain these coefficients. In this method, one expands the force $\partial V/\partial a$

Table V. Description of Crystal Packing for a Set of Minimized Crystals

molecule	unit cell	molecules/ space group	packing motif
	Acids		
1. acetic acid	4	$Pna2_1$	catamer
2. adipic acid	2	$P2_1/c$	chain of dimers
3. α-oxalic acid	4	$Pcab$	catamer
4. β-oxalic acid	2	$P21/c$	chain of dimers
5. butyric acid	4	$C2/m$	cyclic dimers
6. formic acid	4	$Pna2_1$	catamer
7. glutaric acid	4	$I2/a$	twisted chain of dimers
8. malonic acid	2	$P\bar{1}$	twisted dimers
9. methylmalonic acid	2	$P\bar{1}$	chain of dimers
10. propionic acid	4	$P2_1/c$	cyclic dimers
11. valeric acid	4	$P2_1/c$	cyclic dimers
	Amides		
1. oxamide	1	$P1$	sheets of dimers
2. malonamide	8	$P2_1/c$	twisted catamer
3. succinamide	4	$C2/c$	sheets of dimers
4. adipamide	2	$P2/c$	catamer
5. urea	2	$P42_1m$	chain of dimers
6. formamide	4	$P2_1/n$	puckered sheets of dimers
7. *N*-methylacetamide	4	$Pnmm$	catamer
8. diketopiperazine	2	$P2_1/c$	catamer
9. 1,1-dimethyldiketo-piperazine	1	$P1$	chain of dimers
10. cyclopropanecarbox-amide	8	$P2_1/c$	catamer
11. glutaramide	4	$C2/c$	chain of dimers
12. suberamide	4	$C2/c$	planes of dimers

Table VI. Sensitivity Analysis Coefficient $\partial\Delta a/\partial\delta_i$ Associated with the Lattice Vectors for Glutaramide[a]

	sensitivities								
	a			**b**			**c**		
parameter	a_1	a_2	a_3	a_4	a_5	a_6	a_7	a_8	a_9
$\delta_{c'o'}$	2.64	1.61	−1.11	−2.65	−1.66	1.02	0.74	0.26	0.06
$\delta_{hn,n}$	2.31	1.54	−0.05	−2.33	−1.61	0.47	0.93	0.98	0.23

[a] The lattice vectors are given in the Cartesian representation (see text) as the coordinates of the three corners of the cell along the three crystallographic axes **a**, **b**, and **c**.

evaluated at the minimum associated with the potential about the given structural point. Thus,

$$\left.\frac{\partial V}{\partial a}\right|_m = \left.\frac{\partial V}{\partial a}\right|_{exp} + \left.\frac{\partial^2 V}{\partial^2 a}\right|_{exp} \Delta a + \ldots \qquad (11)$$

represents the expansion about the experimental crystal structure. By definition, the left-hand side is null and in the harmonic approximation is

$$\Delta a = -\left[\left.\frac{\partial^2 V}{\partial a\, \partial a}\right|_{exp}\right]^{-1} \left.\frac{\partial V}{\partial a}\right|_{exp} \qquad (12)$$

Use of this approximation makes the calculation feasible since it circumvents the need to relax the crystal in the trial force field at each iteration. However, in addition to the assumption that the experimental structure is similar to the minimum energy structure associated with the potential, the approximation directly relates the curvature of the energy function (with respect to the cell parameters) to the residual. Thus, the size of the residual may be controlled by either the gradient or the curvature, which may have different sensitivities to the parameters. Because of this, the coefficients associated with these observables are more complicated than the other coefficients.

The utility of using these sensitivities to probe the relationship between the structure of the crystal and the underlying potential interaction can be demonstrated by considering the crystals of the amides glutaramide, oxamide, and urea. These crystals serve as convenient representatives of the crystal data set. In a more complete study the detailed analysis carried out on these crystals should be extended to the entire set of crystals.

The crystal structure of glutaramide has four molecules per unit cell that pack according to Figure 8. Each end of the diamide is involved in forming four hydrogen bonds, two along both the **c** and **a** axes. The hydrogen bonds along the **c** axis form dimers, while those along the **a** axis involve two different neighbor molecules. Figure 5 indicates that the unit cell vectors are very sensitive to the hnn bond increment. Table VI shows the coefficients associated with the individual components with respect to this parameter, as well as the c′o′ bond increment, which is also large. In both cases the **a** and **b** vectors have large values relative to the **c** vector, indicating that the hydrogen bond interactions between the dimer chains directed along the **c** axis are less sensitive to changes in the electrostatic interactions that are the interdimer hydrogen bonds. The large sensitivity along **b** is a result of the nonplanarity of the dimer with respect to the **ac** plane. Thus, changes in the hydrogen-bonding interaction between the dimers will cause the chains to rotate about the **c** axis. Furthermore, the increased sensitivity of the **b** vectors should be reflected in increased sensitivity with respect to rotation. This result is also shown in Figure 7.

The oxamide crystal packs with one molecule per unit cell as shown in Figure 9. The molecules form a planar hydrogen-bonded sheet in the **bc** plane separated by 3.1 Å along the **a** axis. The closest intermolecular distance between the sheets is the c′···o′ distance of 2.63 Å. Because this short c′···o′ distance is unique to the oxamide crystal, we expect that the sensitivities associated with this interaction would be larger than the other sensitivity coefficients. In the case of the bond increments we observed an unusually large sensitivity for the unit cell vector, which diminished slightly when the crystal was minimized. Similarly, increases in the unit cell vector coefficient for the c′ and o′ van der Waals radii were also observed. In Table VII the sensitivity for each of the components of the lattice vectors is listed. In all cases the largest coefficient is associated with the **a** axis, which is affected most by changes in the c′···o′ distance. As shown in this table, the distance between the planes is also sensitive to changes in r^*_n. In addition, the components of the **b** axis are more sensitive than those of the **c** axis. As indicated by Figure 9, the oxamide molecules form dimer chains along the **c** axis. Thus, as with the glutaramide crystal, the hydrogen bond interactions between dimer chains are more sensitive to changes in the parameters than are the intrachain interactions.

Finally, we consider the urea crystal (Figure 10). Urea is a particularly interesting amide crystal because each carbonyl ox-

Table VII. Sensitivity Analysis Coefficient $\partial\Delta a/\partial\delta_i$ Associated with the Lattice Vectors for Oxamide[a]

	sensitivities								
	a			**b**			**c**		
parameter	a_1	a_2	a_3	a_4	a_5	a_6	a_7	a_8	a_9
$\delta_{c'o'}$	0.61	−5.05	1.28	3.31	1.51	1.28	−0.77	0.54	−0.13
$r^*_{c'}$	2.83	−15.2	3.72	7.52	4.18	2.25	−0.75	1.01	0.07
$r^*_{o'}$	−6.60	48.8	−10.5	−23.6	−11.6	−5.41	−0.72	−3.96	0.53
$\delta_{hn,n}$	0.247	−1.40	1.61	0.551	0.203	0.349	0.337	−0.158	−0.077
r^*_n	−9.81	71.0	−15.1	−32.2	−16.0	−7.21	0.21	−4.58	1.68

[a] The lattice vectors are given in the Cartesian representation as the coordinates of the three corners of the cell along the three crystallographic axes **a**, **b**, and **c**.

Table VIII. Sensitivity Analysis Coefficient $\partial\Delta a/\partial\delta_i$ Associated with the Lattice Vectors for Urea[a]

	sensitivities								
	a			**b**			**c**		
parameter	a_1	a_2	a_3	a_4	a_5	a_6	a_7	a_8	a_9
$\delta_{c'o'}$	−0.231	−0.096	0.425	−0.097	−0.234	−0.425	−0.116	0.109	−0.142
$\delta_{hn,n}$	0.162	−0.048	−0.004	−0.048	−0.175	−0.008	0.054	−0.057	−0.100

[a] The lattice vectors are given in the Cartesian representation as the coordinates for the three corners of the cell along the three crystallographic axes **a**, **b**, and **c**.

Table IX. Averaged Elementary Sensitivities $\partial \ln V_i/\partial \ln \alpha_j$, $\partial\Delta a_i/\partial \ln \alpha_j$, $\partial F_i/\partial \ln \alpha_j$, and $\partial T_i/\partial \ln \alpha_j$ Associated with the Experimental and Minimized Structures of Carboxylic Acid Crystals

	energy		lattice vectors		force		torque	
	expt	min.	expt	min.	expt	min.	expt	min.
$\delta_{c'o'}$	0.52	0.49	0.31	0.13	7.62	9.14	16.73	22.83
δ_{hoo}	0.37	0.39	0.29	0.14	7.49	7.65	21.61	19.95
δ_{ch}	0.03	0.02	0.05	0.03	0.61	0.60	2.46	2.70
$\delta_{c'h}$	0.08	0.06	0.04	0.02	0.75	0.73	0.68	0.63
$r^*_{c'}$	0.69	0.24	2.05	0.70	26.56	26.25	93.15	58.37
$\epsilon_{c'}$	0.31	0.34	0.23	0.06	5.49	5.44	18.26	11.89
$r^*_{o'}$	1.20	1.09	3.52	1.69	147.76	163.79	303.04	387.75
$\epsilon_{o'}$	0.41	0.40	0.46	0.23	28.03	31.04	57.42	72.19
r^*_{h}	0.13	0.15	1.07	0.57	15.06	14.22	43.30	39.04
ϵ_{h}	0.26	0.25	0.15	0.06	3.05	2.93	0.842	7.66
r^*_{c}	0.34	0.29	0.152	0.71	13.05	13.18	26.49	32.74
ϵ_{c}	0.30	0.29	0.11	0.05	2.61	2.62	5.32	6.42

Table X. Averaged Elementary Sensitivities $\partial \ln V_i/\partial \ln \alpha_j$, $\partial\Delta a_i/\partial \ln \alpha_j$, $\partial F_i/\partial \ln \alpha_j$, and $\partial T_i/\partial \ln \alpha_j$ Associated with the Experimental and Minimized Structures of Amide Crystals

	energy		lattice vectors		force		torque	
	expt	min.	expt	min.	expt	min.	expt	min.
$\delta_{c'o'}$	0.51	0.51	0.967	0.33	2.19	0.246	13.22	12.41
$\delta_{hn,n}$	0.56	0.55	0.40	0.40	4.74	4.81	18.39	18.05
$\delta_{hnn'}$	0.27	0.25	3.28	0.10	2.06	1.81	15.32	9.76
δ_{ch}	0.04	0.03	2.86	0.05	0.47	0.47	4.09	3.80
$\delta_{c'h}$	0.02	0.03	0.05	0.03	1.11	1.09	1.71	1.52
$r^*_{c'}$	0.35	0.31	28.80	1.11	14.89	13.89	96.59	74.37
$\epsilon_{c'}$	0.28	0.29	1.98	0.16	2.91	2.73	18.77	14.74
$r^*_{o'}$	0.66	0.49	54.13	1.36	29.00	29.41	119.48	110.61
$\epsilon_{o'}$	0.15	0.16	5.97	0.21	5.36	5.61	22.88	21.17
r^*_{n}	0.83	0.70	19.67	1.41	37.20	35.20	166.79	160.58
ϵ_{n}	0.22	0.22	1.56	0.22	7.16	7.18	32.14	31.05
r^*_{h}	0.13	0.16	4.13	1.12	19.30	13.71	87.60	73.63
ϵ_{h}	0.22	0.22	0.81	0.20	3.73	2.72	17.03	14.62
r^*_{c}	0.26	0.25	7.30	0.79	9.04	7.97	48.64	47.26
ϵ_{c}	0.27	0.27	0.25	0.06	1.79	1.57	9.81	9.58

ygen is involved in four hydrogen bonds. As shown in the figure, the molecules form hydrogen-bonded ribbons along the axis with the carbonyl oxygen in the plane of and bisecting the n–c′–n angle of the molecule preceding it. These ribbons then pack such that each ribbon hydrogen bonds with two ribbons running perpendicular to it. If we consider the individual components of the lattice vectors (Table VIII) we find that, while the c′o′ and hnn bond increments are involved in hydrogen bonding, their associated sensitivities are very different. In the former, the largest coefficients are the diagonal terms a_1, a_3, and a_9, while in the latter the largest are the a_3 and a_6 terms. This implies that changes in $\delta_{c'o'}$ will lead to a more uniform compression of the crystal in comparison to changes in δ_{hnn}. Again, as noted for the amide crystals, intrachain hydrogen bond interactions are less sensitive to changes in the potential than are interchain interactions.

B. Average Sensitivities. The results in Section A exemplify the type of physical significant information that can be derived from the sensitivity coefficients at the level of individual crystals. By considering the coefficients associated with all the observables in a similar fashion, one can systematically and quantitatively probe for interactions in the potential that lead to deviations in crystal properties. Alternatively, by averaging the coefficients over a set of crystals, information can be gained pertaining to the collective properties of the group and the underlying potential function. Thus, we now consider application of the analysis in terms of the following set of averaged sensitivities:

$$S_{ij}^{\text{rms}} = \sqrt{\frac{1}{N}\sum\left(\frac{\partial(O_j^c - O_j^e)}{\partial \ln \alpha_i}\right)^2} \qquad (13)$$

where the sum is over the set of N crystals. Table IX lists the sensitivity coefficients that were averaged over the amide crystals, and the coefficients averaged over the carboxylic acids are shown in Table X. To further condense the amount of information generated, the sensitivities for the modulus of the rigid-body force and torque, as well as the lattice vectors, were examined instead of the sensitivities associated with the individual components of these observables.

In considering the acids, several general observations can be made. First, the sensitivities corresponding to $r^*_{o'}$ are larger than the other sensitivities. This is true for all the observable calculated for both the experimental and minimum energy crystal structure. Second, only two bond increments, $\delta_{c'o'}$ and δ_{hoo}, have sensitivities that are significant. Of these, $\delta_{c'o'}$ is generally larger than δ_{hoo}. With respect to the other van der Waals parameters, the sensitivities associated with the carbonyl oxygen and carbon are larger. It is interesting to note that the $\partial O/\partial \ln \epsilon_i$ sensitivities are generally

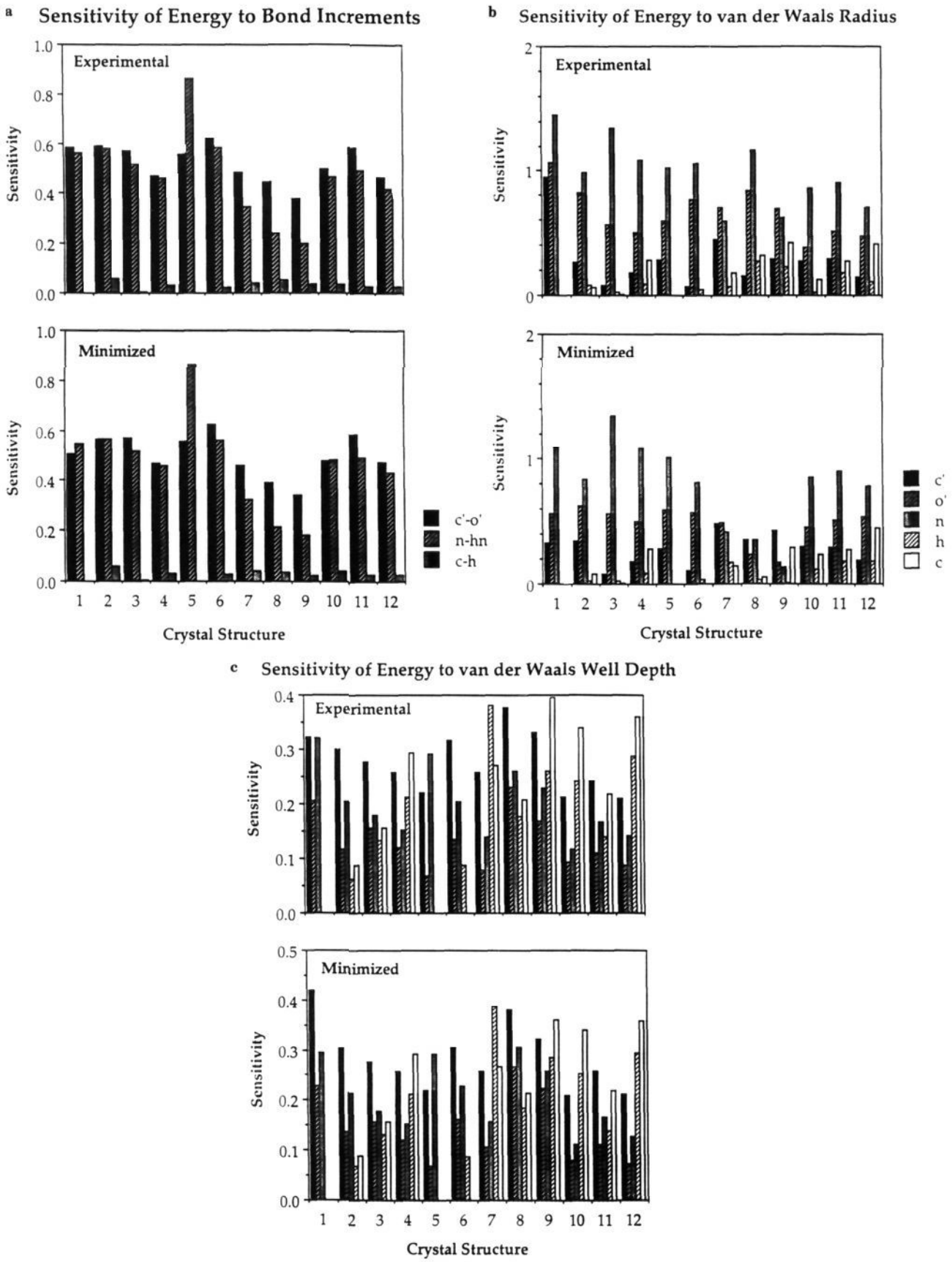

Figure 4. Elementary sensitivities $\partial \ln V_i / \partial \ln \alpha_j$ for the experimental and minimized structures of the amide crystals: (a) sensitivities associated with the bond increments, $\partial \ln V / \partial \ln \delta_{ij}$; (b) sensitivities associated with the van der Waals radii, $\partial \ln V / \partial \ln r_i$; (c) sensitivities associated with the van der Waals well depths, $\partial \ln V / \partial \ln \epsilon_i$. The bond increment for the secondary amide δ_{hnn_j} is included with the primary amide bond increments and the van der Waals constants for the hydrogen bonded to the amide nitrogen hnn are not shown since they were assumed to be zero.

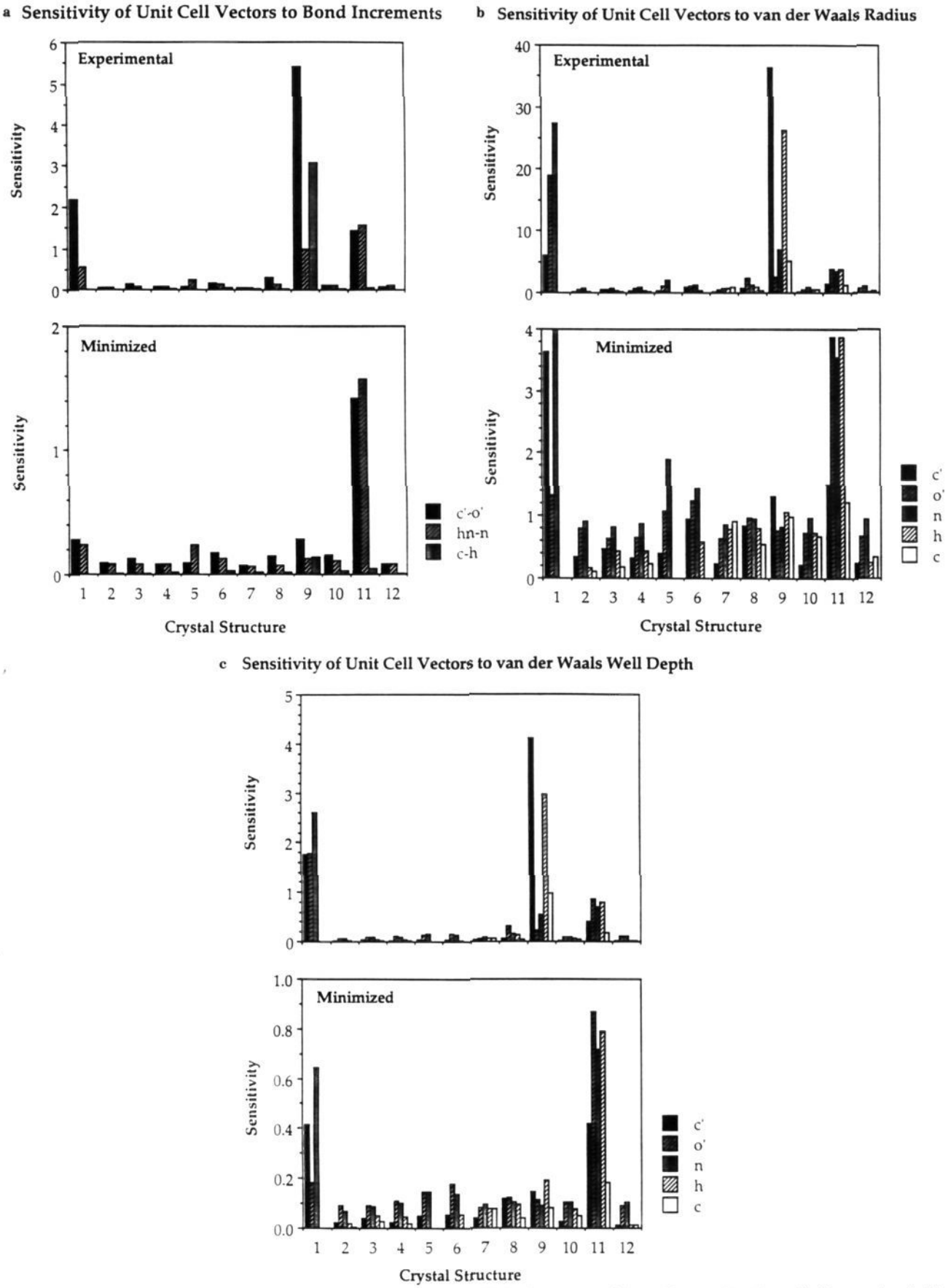

Figure 5. Elementary sensitivities $\partial \Delta a / \partial \ln \alpha_j$ for the experimental and minimized structures of the amide crystals: (a) sensitivities associated with the bond increments, $\partial \Delta a / \partial \ln \delta_{ij}$; (b) sensitivities associated with the van der Waals radii, $\partial \Delta a / \partial \ln r_i$; (c) sensitivities associated with the van der Waals well depths, $\partial \Delta a / \partial \ln \epsilon_i$.

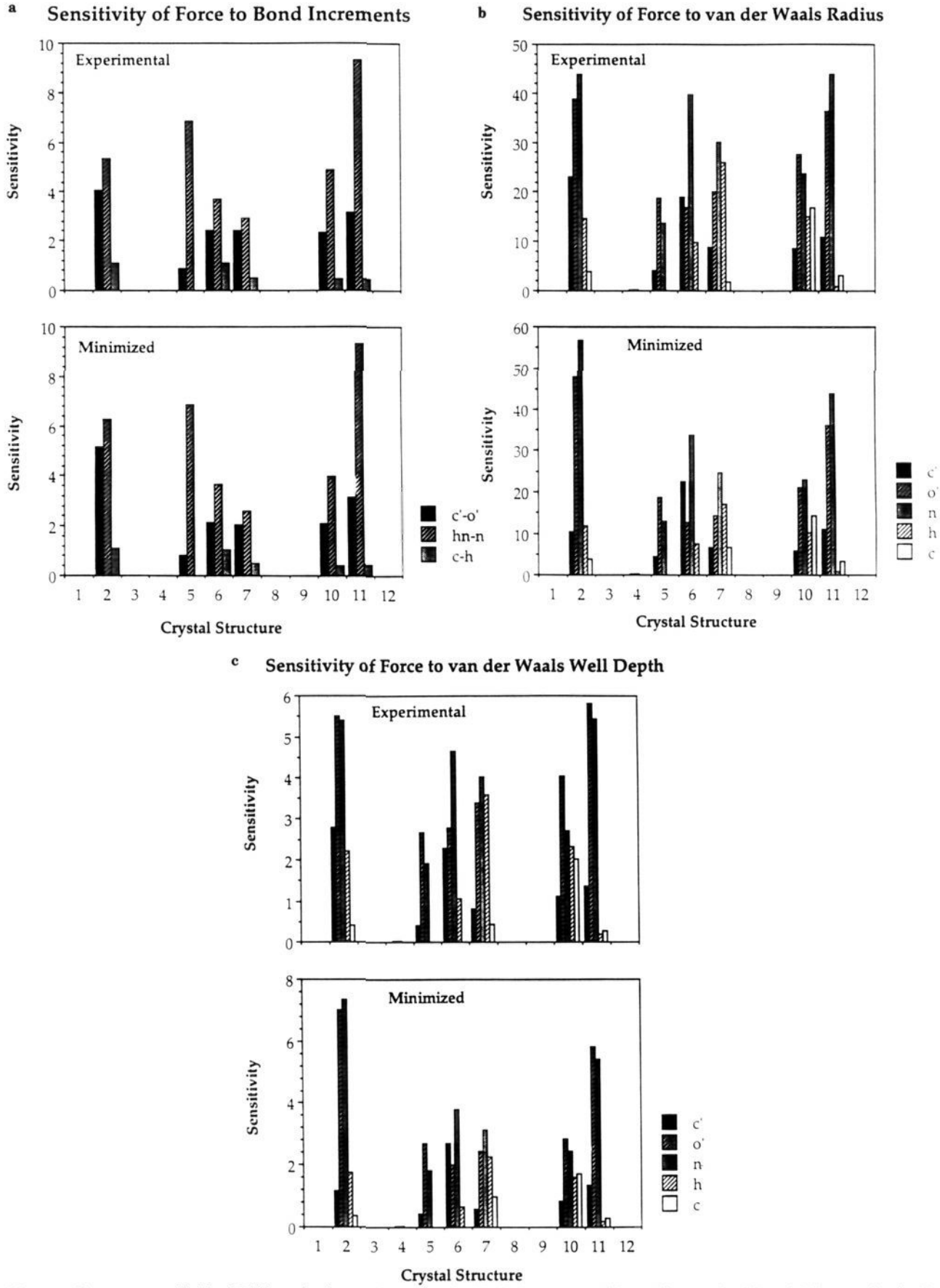

Figure 6. Elementary sensitivities $\partial F_i/\partial \ln \alpha_j$ for the experimental and minimized structures of the amide crystals: (a) sensitivities associated with the bond increments, $\partial F/\partial \ln \delta_{ij}$; (b) sensitivities associated with the van der Waals radii, $\partial F/\partial \ln r_i$; (c) sensitivities associated with the van der Waals well depths, $\partial F/\partial \ln \epsilon_i$.

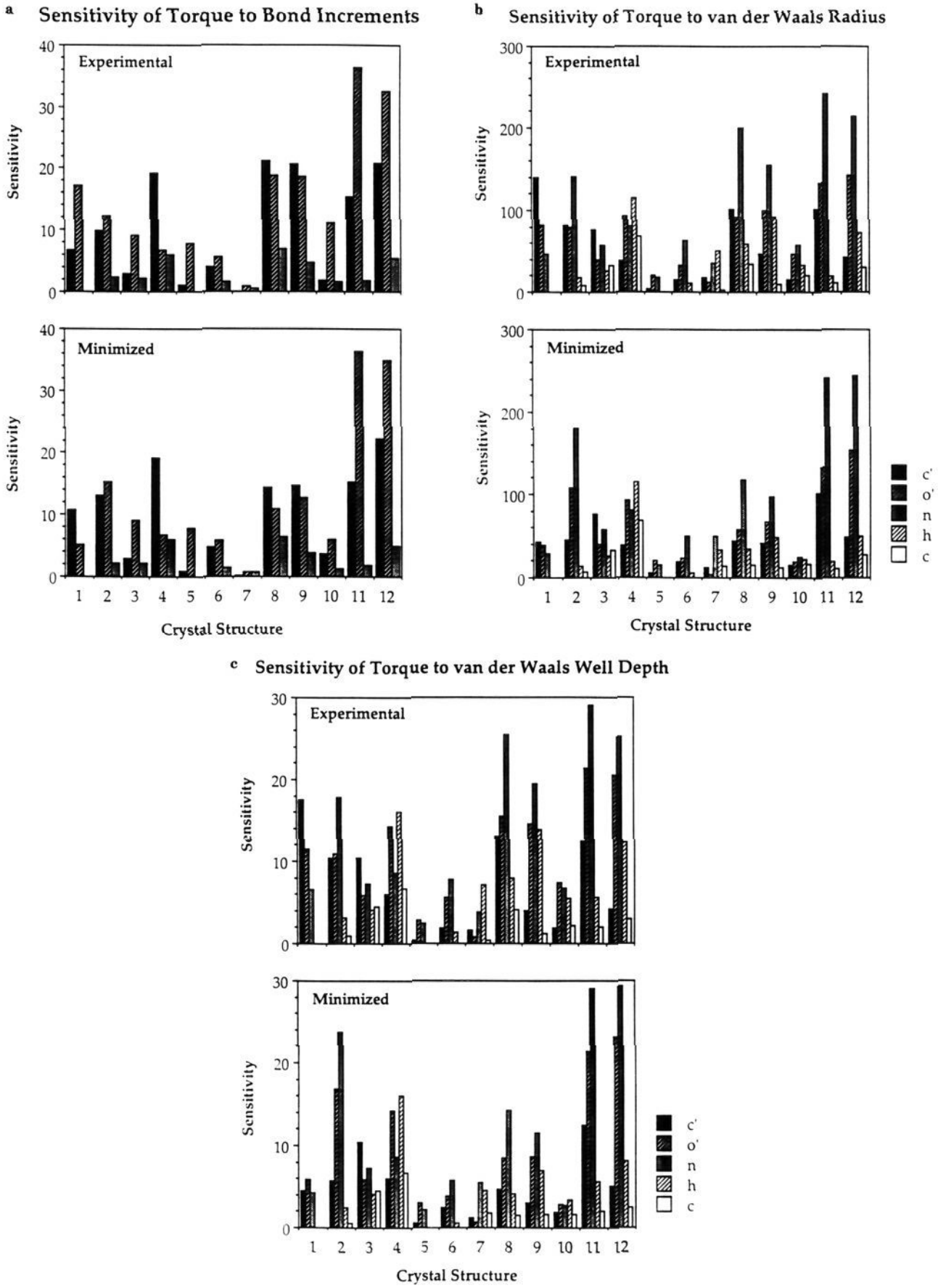

Figure 7. Elementary sensitivities $\partial T_i/\partial \ln \alpha_j$ for the experimental and minimized structures of the amide crystals: (a) sensitivities associated with the bond increments, $\partial T/\partial \ln \delta_{ij}$; (b) sensitivities associated with the van der Waals radii, $\partial T/\partial \ln r_i$; (c) sensitivities associated with the van der Waals well depths, $\partial T/\partial \ln \epsilon_i$.

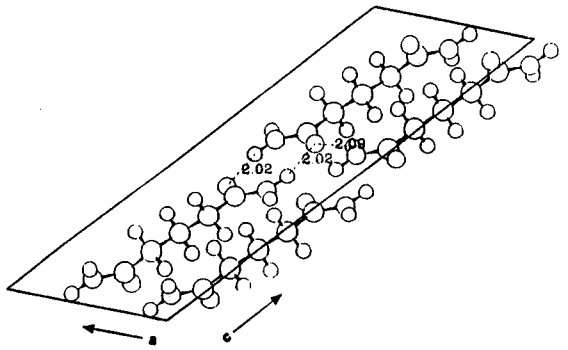

Figure 8. The hydrogen bond structure in the glutaramide crystal viewed along the **b** axis. The intradimer hydrogen bond (2.02 Å) is stronger than the interdimer bond (2.09 Å).

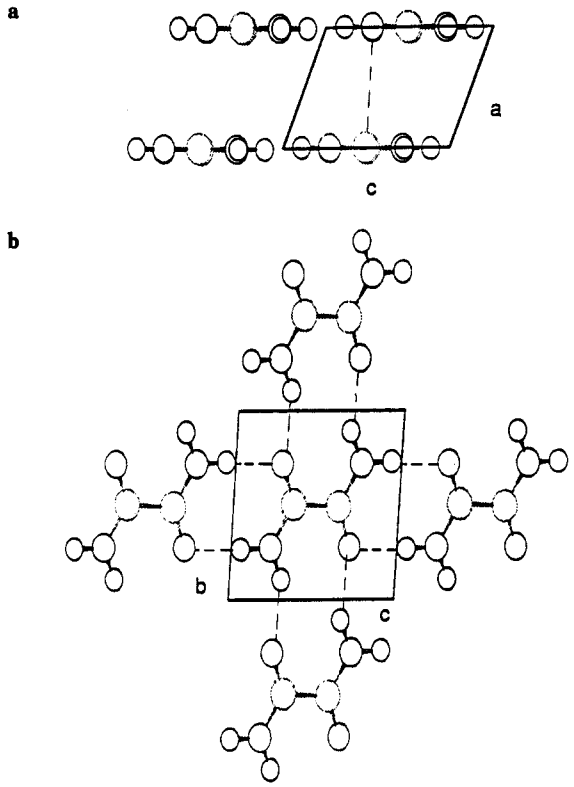

Figure 9. Packing structure of oxamide (a) viewed along the **b** axis to show the cloest intermolecular distance between the carbonyl carbon of one layer and the carbonyl oxygen of the other layer and (b) viewed along the **a** axis to show the extensive hydrogen-bonding network of the crystal layers.

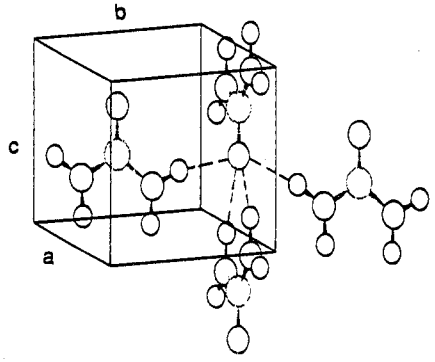

Figure 10. Packing structure of the urea crystal showing the carbonyl oxygen involved in four hydrogen bonds.

smaller than the $\partial O/\partial \ln r^*_i$ sensitivities. The only exception to this trend is displayed by the energy sensitivities when they are calculated for the minimum energy structure. The latter result reflects an increase in the number of interactions located more deeply in the well of the potential after minimization, because the sensitivity of the energy to changes in well depth increases as the interaction distance approaches the bottom of the well.

In general, the qualitative features of the sensitivities do not change whether they are calculated for the experimental configuration or for the minimized structure. This result follows from previous crystal results and the dimer calculations, which showed changes in the trends of the sensitivities with respect to the parameters that occurred only where there were large simultaneous shifts in the associated observables. The only exceptions to this behavior occurred for the lattice vectors. In these cases the sensitivity associated with $\delta_{c'c'}$ was smaller than the δ_{hoo} sensitivity for the minimized structures, while the converse was observed for the experimental structures. In addition to this deviance, the coefficients associated with this property shifted (in some cases dramatically) when the crystal was minimized. For example, the $r^*_{c'}$ sensitivity dropped from 2.05 to 0.70, in contrast to drops from 0.69 to 0.24 and from 93.2 to 58.4 for the energy and torque, respectively. The largest shift in the rigid-body force sensitivities was from 147.76 to 163.79 for the $r^*_{o'}$ parameter. The difference in behavior for these sensitivities is due to the use of the indirect method (eq 12), where subtle changes in the parametric Hessian can cause significant changes in the sensitivities. This conclusion is implied by the relative invariabilities of the rigid-body torque and force when the crystals were minimized.

The same observations that were made with respect to the acids can also be made for the amides. In a comparison of the atom types o', c', and h, common to the two sets of sensitivities, the $\partial a/\partial \ln \alpha_i$ sensitivities were consistently larger for the amides and the shifts in these coefficients upon minimization more noticeable. These shifts brought the two sets of sensitivities into much better agreement in all cases, which was expected, given the similarity of the other sensitivities in the two sets. These results have broad implications in terms of using the harmonic approximation to represent the lattice vector residuals. For the amides, one may be introducing a systematic error into the optimal set of parameters, because the sensitivities of the observable are a manifestation of the approximation used to calculate that property. Clearly, this problem does not occur for the properties that are calculated directly and, for these cases, an accurate description of the relationship between the observable and the underlying potential can be derived without minimizing the crystals.

The above sensitivities provide useful information concerning how the observables used in the least-squares fit are affected by changes in parameters. As has been shown, these quantities are useful in locating parameters that are critical to the value of an observable. By extension, the latter parameters should be defined better through inclusion of the observable in the merit function (eq 1). Another class of sensitivities derived from these coefficients is also very important in revealing the relationship between the choice of observables used in the merit function and the resulting set of optimized parameters. Information concerning this relation is clearly probed by the inverse sensitivities $\partial \alpha_i/\partial O_j^c$ which result from the solution of eq 3:

$$\frac{\partial \alpha}{\partial O^c} = -H^{-1} \frac{\partial^2 R}{\partial \alpha \, \partial O^c} \tag{14}$$

where the Hessian in parameter space is given by

$$H_{ij} = \sum_k^n \sigma_k^2 \left[\frac{\partial r_k}{\partial \alpha_i} \frac{\partial r_k}{\partial \alpha_j} + r_k \frac{\partial^2 r_k}{\partial \alpha_i \partial \alpha_j} \right] \tag{15}$$

The coefficients $\partial \alpha_i/\partial O_j^c$ characterize how changes in the observables affect the value of the parameters. Thus, they are valuable for deducing which type of measurements are most useful for refining a particular parameter. These sensitivities were calculated for each crystal at both the experimental and minimized structures. In the following analysis the atomic A_i and B_i parameters were used instead of r^*_j and ϵ_i because this change facilitated the calculation. As was done with the previous ele-

Table XI. Averaged Inverse Elementary Sensitivity Coefficients $\partial \ln \alpha/\partial \ln V$, $\partial \ln \alpha/\Delta a$, $\partial \ln \alpha/\partial F$, and $\partial \ln \alpha/\partial T$ Associated with the Experimental and Minimized Structures of Carboxylic Acid Crystals

	energy		lattice vectors		force		torque	
	expt	min.	expt	min.	expt	min.	expt	min.
$\delta_{c'o'}$	1.81	1.13	7.05	2.37	2.41	8.72	5.22	2.56
$\delta_{hn,n}$	1.77	1.35	6.24	1.53	2.17	7.48	6.98	2.82
δ_{ch}	2.67	0.64	68.62	60.46	7.59	96.29	50.07	21.12
$\delta_{c'h}$	4.74	0.88	1.30	1.33	3.01	7.58	0.28	0.64
$A_{c'}$	0.21	0.85	0.07	0.91	0.419	3.24	0.043	0.43
$B_{c'}$	2.51	2.44	4.01	20.47	1.29	32.66	4.53	6.88
$A_{o'}$	0.27	0.38	0.05	0.37	0.431	1.51	0.053	0.18
$B_{o'}$	0.28	0.39	1.06	5.00	0.371	8.82	1.39	1.71
A_n	0.42	0.35	0.33	28.58	0.964	44.63	0.28	9.60
B_n	3.60	8.19	3.75	153.45	2.51	240.60	2.02	51.64
A_c	0.26	0.23	0.06	7.47	0.102	10.94	0.02	2.36
B_c	2.81	13.66	4.30	51.58	3.41	88.39	2.88	17.71

Table XII. Averaged Inverse Elementary Sensitivity Coefficients $\partial \ln \alpha/\partial \ln V$, $\partial \ln \alpha/\Delta a$, $\partial \ln \alpha/\partial F$, and $\partial \ln \alpha/\partial T$ Associated with the Experimental and Minimized Structures of Amide Crystals

	energy		lattice vectors		force		torque	
	expt	min.	expt	min.	expt	min.	expt	min.
$\delta_{c'o'}$	1.54	2.35	1.80	1.44	2.04	4.29	0.348	1.88
δ_{hnn}	0.82	1.73	0.34	1.42	0.72	0.45	0.167	0.77
$\delta_{hnn'}$	0.53	13.68	1.40	4.27	3.84	7.96	0.395	4.0
δ_{ch}	3.18	17.51	1.79	6.62	3.23	6.25	0.807	6.88
$\delta_{c'h}$	4.76	9.33	0.75	2.05	0.74	3.22	0.112	0.41
$A_{c'}$	0.81	0.78	0.35	0.41	0.56	0.49	0.093	0.36
$B_{c'}$	4.79	4.08	1.08	2.39	2.69	1.58	0.361	2.88
$A_{o'}$	0.39	0.98	0.51	0.78	1.50	0.68	0.178	0.33
$B_{o'}$	1.42	0.82	1.37	2.09	2.75	0.68	0.331	1.41
A_n	0.10	0.26	0.64	0.35	0.42	0.18	0.082	0.17
B_n	1.21	2.05	1.06	2.06	0.57	0.77	0.147	0.79
A_h	2.13	3.81	0.20	0.91	0.45	1.03	0.308	1.04
B_h	7.76	14.03	0.95	5.32	0.54	1.38	1.10	4.63
A_c	0.70	1.47	0.55	0.24	1.36	0.21	2.14	0.19
B_c	7.98	21.41	0.86	6.47	1.84	1.27	0.806	6.44

mentary sensitivities, the coefficients were then averaged over the amide and acid crystals with use of eq 13. The resulting averages are shown in Tables XI and XII.

The sensitivities associated with the B_i parameters are uniformly larger than those corresponding to the A_i coefficients for all observables, indicating that including more sublimation energies or crystal structures preferentially improves the fit of the dispersive term. In this regard, $B_{o'}$ will not be further refined by adding more observables relative to the other dispersive parameters, since the coefficients are generally smaller for this parameter. This result was anticipated since the carboxylic and hydroxyl oxygens are described by the same van der Waals parameters. This equivalence effectively increases the number of short intermolecular distances in the acid crystals, which constrain the values for $r^*_{o'}$ and $\epsilon_{o'}$. Furthermore, it introduces o'···o distances that are not sampled by the o'···o' and o···o interactions. In contrast to this situation, the bond increment δ_{ch} parameters will be significantly better defined with the addition of more structural data. This is especially true for the lattice vectors and the torque observables, where the $\partial \ln \delta_{ch}/\partial O_i$ sensitivities are almost an order of magnitude greater than the other $\partial \ln \alpha_j/\partial O_i$ sensitivities. With respect to the other repulsive terms, the sensitivities associated with the aliphatic hydrogens are larger. While this difference is small for some of the observables (i.e., the energy), this trend is noted for all the observables. Thus, increasing the number of observables, especially the rigid-body force, should help define the hydrogen-repulsive term. This observation illustrates the usefulness of the analysis, since it was not expected. On the basis of the distribution of short intermolecular distances for the c···h interaction in the acid crystals, one would expect that these parameters should be well-defined. However, the sensitivities inherently contain information about the importance of this specific interaction in determining the observables, which are then reflected in the magnitude of the coefficients. Thus, in spite of the increased number of short interactions, the sensitivities are high because the packing structure and lattice energy are dominated by the hydrogen bond interaction. The conclusion that follows is that this set of crystals should be augmented with non-hydrogen bonding crystals.

The sensitivity coefficients for the minimized configuration were very different from those calculated at the experimental configuration. In most cases the sensitivities increased in magnitude. This difference reflects a shift in both the elements of the second derivatives in eq 15, as well as the differences between the observables and the calculated values. In general, one expects that the differences predicted by the residual r_i at the end of the optimization should underestimate the true differences determined when the crystals are minimized. Thus, one expects that the contribution from the second term in eq 15 should increase.

Similar observations were noted for the amide sensitivity coefficients. Again, relative to the other van der Waals coefficients the c', h, and c dispersive terms should gain the most with the inclusion of lattice energies. It was found that the sensitivities $\partial \ln r^*_i/\partial O^c_i$ were relatively small, indicating that this parameter is rather insensitive to changes in the observables. This was especially true for the lattice energies. As before, the sensitivities for the minimized structures were significantly different from the ones evaluated at the experimental structure. One noticeable trend that stands out is that the sensitivities associated with the secondary amide are much larger than those of the primary amide. This difference is a reflection of the scarcity of secondary amide crystals in the data sets relative to the number of primary crystals.

A special class of derived sensitivities may be achieved by utilizing the previous sensitivities via the following expression:[12]

$$\frac{\partial O_i}{\partial O^c_j} = \sum_k \frac{\partial \alpha_k}{\partial O^c_j} \frac{\partial O_i}{\partial \alpha_k} \tag{16}$$

These sensitivities characterize the dependence of the calculated value of an observable on the values of the experimental observables included in the fit. These sensitivities are relevant when addressing the issue of the importance of using a set of observables to define the parameters. An example is whether inclusion of the rigid-body forces and torques helps define the ability to predict crystal sublimation energies. When O^c_i is not used in the merit function, the sensitivities yield information applicable to assessing the potential's ability to predict observables that are not used in the optimization. As an illustration of the type of information yielded by these coefficients, a comparison of the sensitivities for the two crystal forms of oxalic acid is shown in Table XIII. Oxalic acid packs in a crystal either as a ribbon of hydrogen-bonded dimers (β form) or as a catamer (α form). Although the hydrogen bonds in the former are stronger, the latter form is the lower-energy structure by 1.3 kcal/mol.[17] The table shows that the calculated lattice energies for the acid crystals were all more sensitive to changes in the observed lattice energy for the β form than the α form. This could in part be due to the prevalence of the dimer structure in the crystals (see Table V). However, the similarity of the crystal structures does not explain the fact that the larger sensitivities for formic acid (catamer) and malonic acid (dimer) were seen for the β and α forms, respectively. In this

Table XIII. Comparison of Sensitivities $\partial \ln V_j/\partial \ln V^e(\alpha\text{-oxalic acid})$ and $\partial \ln V_j/\partial \ln V^e(\beta\text{-oxalic acid})$ for the Carboxylic Acid Crystals Evaluated at the Experimental Configuration[a]

carboxylic acid	form of oxalic acid	
	α	β
acetic acid	0.48	0.67
adipic acid	0.43	0.65
α-oxalic acid	1.0	0.89
β-oxalic acid	0.92	1.0
butaric acid	0.34	0.54
formic acid	0.73	1.0
glutaric acid	0.44	0.69
malonic acid	0.57	0.80
methylmalonic acid	0.38	0.69
propionic acid	0.34	0.61
valeric acid	0.32	0.52

[a] V_j and V^e are the calculated lattice energy for the jth carboxylic acid crystal and the experimental lattice energy for the α and β crystalline form of oxalic acid.

manner the coefficients uncover relationships that are not intuitively apparent.

Conclusion

Until recently, the primary focus of the increased interest in molecular mechanics and dynamics has been toward its application and not toward the underpinnings of the generation of more accurate potential energy functions. Now, with more appreciation of the importance of the latter issue, activity in this area has developed, along with a need to approach it in a systematic manner. In this paper we have reported on the application of sensitivity analysis to the derivation of intermolecular parameters from experimental crystal data. These coefficients have proven to be valuable in elucidating the relationship between the optimized potential function and the observables used in the fitting procedure. The first class of sensitivities studied was that of the elemental sensitivities $\partial O_i/\partial \ln \alpha_j$, which proved to be useful in determining the relative importance of a parameter in defining the value of a specific observable. This information is useful for probing where changes in the potential can be made, to reduce the residual sum of squares. As an example of the former, they could be used to locate interactions that are pivotal to the binding of a substrate to an enzyme. This would be done by calculating the parametric sensitivities of important distances defining the enzyme–substrate complex and then identifying the largest sensitivities associated with these distances. In addition, when the observables are torques and forces, the coefficients specify which parameters are important in causing structural shifts away from a given conformation. This feature is also important for understanding structure–function and structure–property issues. In addition to using the elemental sensitivities to analyze the relationship between the observable and potential parameters, the derived coefficients were also shown to be valuable for understanding their relationship. These quantities are used to directly probe the questions of which observables are necessary to determine a specific parameter and what new experiments would be useful to augment the available set.

The present paper has not attempted to close the loop on potential improvement by implementing the suggestions revealed by the sensitivities. Rather, the purpose of this paper was to illustrate the type and quality of information available from performing a sensitivity analysis. The loop will be closed in a following paper.

Acknowledgment. The support of this work by the National Institutes of Health is gratefully acknowledged. In addition, one of the authors (H.R.) would like to acknowledge partial support for this research from the Squibb Institute for Medical Research and the Office of Naval Research.

Intrazeolite Carbonyl(η^5-cyclopentadienyl)dihydridoiridium(III) ($CpIr(CO)H_2$–$M_{56}Y$, Where M = H, Li, Na, K, Rb, and Cs)

Linda Crowfoot, Geoffrey A. Ozin,* and Saim Özkar†

Contribution from Lash Miller Chemistry Laboratories, University of Toronto, 80 Saint George Street, Toronto, Ontario, Canada M5S 1A1. *Received June 4, 1990*

Abstract: Vapor-phase impregnation and thermal equilibration of $CpIr(CO)H_2$ in dehydrated $M_{56}Y$ (where M = H, Li, Na, K, Rb, and Cs) yields samples in which the guest displays two main anchoring modes. In $Li_{56}Y$ and $Na_{56}Y$, a $CpIrH_2(CO)\cdots M^+$ interaction is favored (type I), whereas in $K_{56}Y$, $Rb_{56}Y$, and $Cs_{56}Y$ the preferred-binding geometry involves $CpIr(CO)H_2\cdots M^+$ (type II). The topology, spacial requirements, and ionic potential of the site II M^+ cations appear to be mutually responsible for "lock-and-key" anchoring effects of $CpIr(CO)H_2$ in the supercage of zeolite Y. The thermal and photochemical reactivities of $CpIr(CO)H_2$–$M_{56}Y$ toward D_2, HBr, CO, C_6H_6, and alkanes are investigated and compared with the situation known in solution. With D_2, one finds only H/D exchange of the hydride ligands to yield intrazeolite $CpIr(CO)D_2$–$M_{56}Y$ without hydride or Cp ring hydrogen scrambling, while exposure to CO yields the known intrazeolite species $CpIr(CO)_2$–$M_{56}Y$. In the case of both Brønsted acid $H_{56}Y$ and proton-loaded $(HBr)_8$–$Na_{56}Y$ zeolites, one discovers a proton-induced, reductive-elimination, dimerization reaction, which yields the novel intrazeolite dimer $Cp_2Ir_2(CO)_2$–$M_{56}Y$ anchored to a supercage Brønsted acid site via one of its bridge carbonyl ligands. By contrast to the situation found in solution, $CpIr(CO)H_2$–$M_{56}Y$ so far appears to be photochemically and thermally inactive toward C–H bond activation chemistry with arenes and alkanes.

Introduction

Species of the type $CpIrLH_2$ (where L = CO and PR_3) have evoked much interest in solution-phase organometallic chemistry and homogeneous catalysis mainly because of their ability to participate in reactions of the type illustrated in Scheme I.[1,2] In 1982, Janowicz and Bergman discovered that photolysis of $Cp^*Ir(PMe_3)H_2$ in the presence of alkanes yields the C–H bond inserted product $Cp^*Ir(PMe_3)(R)H$.[3] After the reported synthesis

† On leave of absence from the Chemistry Department, Middle East Technical University, Ankara, Turkey.

(1) Spousler, M. B.; Weiller, B. H.; Stoutland, P. O.; Bergman, R. G. *J. Am. Chem. Soc.* **1989**, *111*, 6841 and references cited therein.
(2) Heinekey, D. M.; Millar, J. M.; Koetzle, T. F.; Payne, N. G.; Zilm, K. W. *J. Am. Chem. Soc.* **1990**, *112*, 909 and references cited therein.

0002-7863/91/1513-2033$02.50/0